Hydrogen Chemisorption on Al_2O_3-Supported Gold Catalysts

Eveline Bus, Jeffrey T. Miller,† and Jeroen A. van Bokhoven*

Institute for Chemical and Bioengineering, Swiss Federal Institute of Technology, ETH, CH-8093 Zurich, Switzerland

Received: April 1, 2005; In Final Form: June 1, 2005

Hydrogen is dissociatively adsorbed on the gold particles in Au/Al_2O_3 catalysts, as demonstrated by a combination of in-situ X-ray absorption spectroscopy, chemisorption, and H/D exchange experiments. This chemisorption of hydrogen induces changes in the Au L_3 and L_2 X-ray absorption near-edge structures. The gold atoms on corner and edge positions dissociate the hydrogen, which does not spill over to the face sites. Therefore, the average number of adsorbed hydrogen atoms per surface gold atom increases with decreasing particle size. With temperature, the hydrogen uptake by supported gold increases or remains constant, whereas it decreases for platinum. Furthermore, in H/D exchange experiments, the activity of Au/Al_2O_3 increases strongly with temperature. Thus, the dissociation and adsorption of hydrogen on gold is activated.

Introduction

Bulk gold is the least active metal in the adsorption of atoms and molecules,[1] but its properties change remarkably when it is highly dispersed and supported on a metal oxide.[2] These supported gold nanoparticles catalyze the oxidation of CO, the epoxidation of propylene, and the low-temperature WGS reaction.[2,3] For the most part, oxidation reactions have been studied.[2−4] Gold, however, is also active in reactions involving hydrogen, such as hydrogenation of alkenes, alkadienes, alkynes, and ketones, as well as in hydrogenolysis and in dehydrogenation reactions, as reviewed by Bond and Thompson.[3] The selective hydrogenation of hydrocarbons with more than one unsaturated bond is of particular interest. Acetylene,[5] 1,3-butadiene, crotonaldehyde, acrolein,[6−8] and other α,β-unsaturated aldehydes[9,10] are selectively hydrogenated by supported gold nanoparticles. Despite hydrogen being an important reactant in these reactions, there are only few studies dealing with the interaction of gold and hydrogen. On Au(110)(1 × 2), no chemisorption of hydrogen molecules was observed. Hydrogen atoms adsorb on this Au surface and desorb again at 226 K.[11] Stobiński et al.[12] showed that hydrogen molecules chemisorb dissociatively on thin, unsintered gold films and suggested that hydrogen reacts with gold atoms on corners and edges. The hydrogen coverage was less than 0.015 at a pressure of 0.3 Pa and a temperature of 78 K. Okada et al.[13] found that hydrogen molecules adsorb dissociatively on thin Au films grown on an Ir(111) surface. They attributed this to localized sites such as defects and relaxed structures. These results show that, under certain conditions, hydrogen chemisorbs on the surface of gold. However, these studies were performed under conditions and with structures that differ from those in supported gold catalysis. Chemisorption of hydrogen by supported gold has been occasionally mentioned, and some or no chemisorbed hydrogen has been reported.[3] Lin and Vannice[14] did not find measurable amounts of chemisorbed hydrogen on Au/SiO_2 and Au/TiO_2 at 298 K. At 473 K, one Au/TiO_2 sample adsorbed a small amount of hydrogen of about 1 atom-% of the amount of gold. These authors suggested that, for this catalyst, the adsorption process is activated and that the hydrogen is dissociated. In their samples, the gold particle size was around 30 nm, which is too big to show catalytic activity.[2] Jia et al.[5] measured a H/Au of 14% for 3.8-nm Au particles on Al_2O_3, and this catalyst was active in the acetylene hydrogenation. Because the activity of gold catalysts in hydrogenation reactions suggests the dissociative adsorption of hydrogen, our goal is to gain insight into the chemisorption of hydrogen on supported gold nanoparticles under catalytically relevant conditions by studying chemisorption and the Au−H interaction.

To determine whether the hydrogen is chemisorbed on the gold particles, the Au−H bond must be observed. This can be achieved with X-ray absorption spectroscopy (XAS). It is well established that the chemisorption of hydrogen induces significant changes in the Pt L_2 and L_3 X-ray absorption near-edge structures (XANES) of supported Pt particles.[15−31] Here, we report a very similar change in the Au L_2 and L_3 XANES. Quantitative measurements of the adsorption of hydrogen have been performed in the temperature range 298−523 K, and the hydrogen uptake is compared with that of Pt/SiO_2. To determine whether dissociation of hydrogen takes place, H/D exchange experiments were performed.

Experimental Section

Sample Preparation and Characterization. Gold particles supported on γ-Al_2O_3 were prepared by adsorbing $HAuCl_4$ on a γ-Al_2O_3 support (Condea or Catalpal, pore volume 0.5 cm^3/g, specific surface area 230 m^2/g) by incipient wetness impregnation with an aqueous solution or by deposition−precipitation. In the deposition−precipitation method, 50 mL of an aqueous solution containing 0.8 g $HAuCl_4$ was added to a slurry of 20 g Al_2O_3 in 300 mL water. The pH was adjusted to 4 with HNO_3 and subsequently the solution was stirred at room temperature. The resulting yellow powder was recovered by filtering and washing with water. In both methods, chlorine was removed by stirring the $AuCl_x/Al_2O_3$ powder in 10 mL water per gram powder at 343 K and maintaining a pH of 8 using NaOH. The resulting white powder was dried at 363 K and stored in the dark. The initial gold content in the sample

* Author to whom correspondence should be addressed. Phone: +41-1-632-5542; fax: +41-1-632-1162; e-mail: j.a.vanbokhoven@chem.ethz.ch.
† BP Research Center, E-1F, Naperville, IL 60563.

10.1021/jp051660z CCC: $30.25
Published on Web 07/07/2005

TABLE 1: Particle Sizes as Determined with STEM and EXAFS

	metal loading (wt %)	particle size (nm) STEM	EXAFS
Pt/SiO_2-A[a]	1.0	2	1.2
Pt/SiO_2-B[b]	1.0	20	5
Au/Al_2O_3-A[c]	0.58	1.2	n.d.[d]
Au/Al_2O_3-B[c]	0.92	3	n.d.
Au/Al_2O_3-C[c]	1.21	10	1.3
Au/Al_2O_3-D[e]	0.43	1.4	1.1
Au/Al_2O_3-E[e,f]	0.43	2	n.d.

[a] Prereduced at 423 K. [b] Prereduced at 873 K. [c] Prepared by deposition−precipitation. [d] n.d. = not determined. [e] Prepared by incipient wetness impregnation. [f] Au/Al_2O_3-E is Au/Al_2O_3-D reduced at 673 K.

prepared by impregnation was 2 wt %, and after the treatment with base, it was 0.43 wt %. The gold content varied from 0.4 to 1.2 wt %. It was determined by atomic absorption spectrometry (AAS) on a Varian SpectrAA instrument after dissolving the samples in concentrated HF and HNO_3 or by inductively coupled plasma spectrometry after dissolving in HF. The chlorine content in all the samples was negligible, as confirmed with X-ray fluorescence. The samples were reduced at 473 K, with the exception of Au/Al_2O_3-E, which was reduced at 673 K (Table 1). The reduction and metal particle formation were done prior to analysis. Pt/SiO_2 was prepared by adding an aqueous solution of tetraammine platinum nitrate (PTA) to a slurry of SiO_2 (Davison 644, pore volume 1 cm^3/g, specific surface area 290 m^2/g) in an NH_4OH solution with a pH of 10. After adsorption of the PTA, the powder was filtered, washed, and dried at 373 K. The 1 wt % Pt/SiO_2 samples were prereduced at 423 K (Pt/SiO_2-A) or 873 K (Pt/SiO_2-B).

The metal particle size was determined by extended X-ray absorption fine structure analysis (EXAFS, see XAS section) and by scanning transmission electron microscopy (STEM). For STEM, the material was dispersed in ethanol and was deposited onto a perforated carbon foil supported on a copper grid. The investigations were performed with a Tecnai F30 microscope operating with a field emission cathode at 300 kV. STEM images, obtained with a high-angle annular dark-field detector, reveal the metal particles with a bright contrast (Z contrast). The images were taken after using the samples in the hydrogen chemisorption experiments.

X-ray Absorption Spectroscopy (XAS). The sample was pressed into a self-supporting wafer and was placed in a stainless-steel in-situ cell.[18] The cell was connected to a gas-flow system, temperature controller, and vacuum pump. The XAS experiments were performed at beamline X1 of HASYLAB (Hamburg, Germany) and at the SNBL (BM01B) and DUBBLE (BM26A) stations at the ESRF (Grenoble, France). At beamline X1, the double-crystal monochromator was equipped with Si(111) crystals that were detuned to 70% to remove higher harmonics. At the SNBL, the incident X-rays were monochromated by a Si(111) channel-cut monochromator, and harmonics were rejected by a chromium-coated mirror. At the DUBBLE station, a double-crystal monochromator was used, followed by two vertically focusing Pt- and Si-coated mirrors to reject the harmonics. All the spectra were recorded in transmission mode using ion chambers for detection. Prior to measurement, the samples were reduced at 473 K in a 20 mL/min H_2 flow and were cooled in this flow to 298 K. At this temperature, XAS data for the L_3 and L_2 edges were collected in static hydrogen atmosphere. Subsequently, the cell was evacuated at 473 K for 2 h to remove the adsorbed hydrogen. L_3 and L_2 XAS spectra were collected in dynamic vacuum ($<10^{-2}$ Pa) at 298 K.

XAS data analysis was carried out using the XDAP software package.[32] The absorption data were pre-edge- and background-subtracted by means of standard procedures.[33] The spectra were normalized on the height of the edge-step at 50 eV over the edge. Multiple shell fitting was performed in *R*-space ($1.5 < R < 3.5$ Å, $3 < k < 12$ $Å^{-1}$) using a *k* weighting of 3. Although surface atoms may vibrate anharmonically or there can be an asymmetric distribution of distances, symmetric distributions were assumed in the fitting. Experimentally calibrated theoretical references of gold and platinum foils, Au_2O_3, and PtO_2 obtained with the FEFF8 code[34] were used.

The pre-edge-subtracted and normalized XANES spectra were aligned to remove initial state core level shifts and final state screening effects.[24] The L_2 edges measured in hydrogen and in a vacuum have the same shape at the onset and, thus, were aligned on this onset. Ramaker et al.[24] state that, after alignment, the Pt L_2 edges overlay each other over about 60% of the height of the edge-step and therefore align the L_2 edges on 0.6 of their step height. This does not lead to a proper alignment of the Au L_2 edges, because their shape differs from that of the Pt L_2 edges. A good alignment of the Au L_2 edges was obtained by aligning them on 0.4 of their step height. This also gave good alignment of the Pt L_2 edges; thus, the same procedure was used for Pt. The energy of the point in the L_2 edges having an intensity of 0.4 was set to zero. The L_3 EXAFS oscillations were then aligned on the L_2 EXAFS oscillations measured under the same conditions, between 50 and 120 eV over the edge, by means of a least-squares method.

Hydrogen Chemisorption. Hydrogen chemisorption analyses were performed under static volumetric conditions with a Micromeritics ASAP 2010 apparatus. We checked that the supports did not adsorb hydrogen. The procedure for the chemisorption experiments was similar to that of the XAS experiments. The samples were reduced at 473 K (with the exception of Au/Al_2O_3-E, which was reduced at 673 K), evacuated at 473 K for 2 h, and left to cool to the temperature of the analysis. Analyses were done from 298 to 523 K. The first adsorption isotherm was obtained by measuring the adsorbed amount of hydrogen for pressures from 1 to 100 kPa. The total amount of adsorbed hydrogen was obtained by extrapolating the linear high-pressure part ($10 < P < 100$ kPa) of the isotherm to zero pressure. From this, the hydrogen/metal (H/M) value for the total adsorption was calculated, which is the ratio of the number of adsorbed hydrogen atoms to the total number of metal atoms multiplied by 100%. After completing the first adsorption isotherm, the weakly adsorbed hydrogen was removed by evacuating for 2 h at the analysis temperature. A second isotherm was measured and the amount of strongly adsorbed hydrogen was determined by taking the difference between the first and second adsorption isotherm. Each measurement was performed three times and the average H/M value was used.

H/D Exchange. Hydrogen/deuterium (H/D) exchange experiments were carried out in a standard flow reactor at 298 and 373 K. The flow over the reactor was 10 mL/min. The feed gas consisted of 2 mL/min H_2 and 2 mL/min D_2; the makeup gas was argon. Pelletized catalyst (50 mg) with a mesh size of 250−300 μm was used. The catalyst bed was in the middle part of a quartz tube reactor with 4-mm inner diameter and was held in place by quartz wool. Prior to catalytic tests, the catalyst was reduced in 10 mL/min pure H_2 at 473 K for 1 h. Mass spectrometry was used to detect H_2, HD, and D_2. Small amounts of HD formed in the experimental setup without catalyst, and the product concentrations were corrected for this. The HD con-

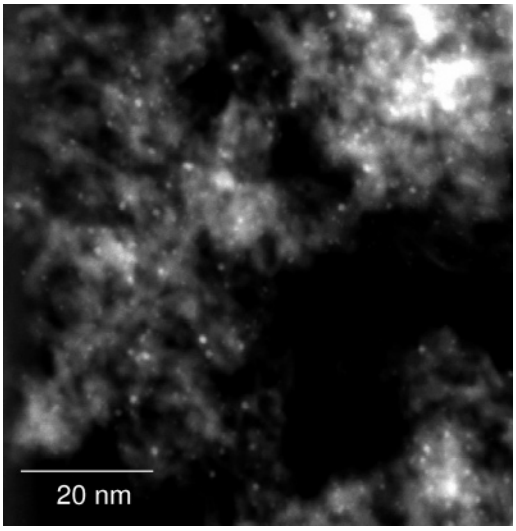

Figure 1. Typical STEM image of supported Au/Al_2O_3-D catalyst.

centration is expressed as the ratio of the amount of HD (in mL/min) to the total amount of H_2, D_2, and HD (4 mL/min) multiplied by 100% and has a maximum of 47%. The approach to equilibrium (η) is defined as the quotient of the reaction quotient and the equilibrium constant

$$H_2 + D_2 \leftrightarrows 2HD$$

$$\eta = \frac{[HD]^2}{[H_2][D_2]} \times \frac{1}{K_{eq}} \quad (1)$$

where K_{eq} is the equilibrium constant of 3.2,[3] which gives

$$\eta = \frac{[HD]^2}{[H_2][D_2]} \times \frac{1}{3.2} = \frac{1.25 \times [HD]^2}{(100 - [HD])^2} \quad (2)$$

With this equation, the approach to equilibrium can be deducted directly from the HD concentration in the product mixture. The value of $(1 - \eta)$ is the fractional distance from equilibrium. Thus, net turnover frequencies (TOF) can be expressed as

$$TOF_{net} = TOF_{forward} \times (1 - \eta) \quad (3)$$

from which forward TOFs can be obtained

$$TOF_{forward} = TOF_{net}/(1 - \eta) \quad (4)$$

The forward turnover frequencies are calculated from the moles of HD in the product feed per mole of available metal atom per minute. Two TOFs are calculated: one per metal surface atom, as determined from the particle size found by STEM and EXAFS, and one per hydrogen-adsorbing metal atom, as determined in the hydrogen chemisorption experiments.

Results

Particle Size from STEM and EXAFS. Table 1 lists the particle sizes of the samples, as determined by STEM and EXAFS. With metal loadings up to 1 wt % and reduction temperatures not exceeding 473 K, particles of 1−3 nm were obtained. The particle size distribution was narrow, as found with STEM (Figure 1). Higher reduction temperatures (873 K for Pt/SiO_2-B) and increased loadings (1.2 wt % for Au/Al_2O_3-C) led to bigger particles and a broader particle size distribution. The particle sizes found with EXAFS and STEM coincide for the small particle sizes. For bigger particles (Pt/SiO_2-B and Au/Al_2O_3-C), a larger particle size is determined with STEM than with EXAFS.

TABLE 2: Results of the First-Shell EXAFS Analyses[a]

sample	conditions	CN[b]	ΔR (Å)[c]	$\Delta\sigma^2$ (10^{-4} Å^2)	ΔE_0 (eV)
Pt/SiO_2-A	in a vacuum	7.8	−0.06	40	1.4
	in hydrogen	8.6	−0.01	12	0.4
Pt/SiO_2-B	in a vacuum	11	0	4	−1.8
	in hydrogen[d]	9.7	−0.02	−11	1.7
Au/Al_2O_3-C	in a vacuum[d]	7.6	−0.07	85	−3.6
	in hydrogen[d]	7.5	−0.08	84	−2.8
Au/Al_2O_3-D	in a vacuum	6.4	−0.09	57	−2.1
	in hydrogen	6.6	−0.09	48	−2.2

[a] $1.5 < R < 3.5$ Å, $3 < k < 12$ Å^{-1}, k^3 weighting. [b] Pt−Pt coordination number for Pt/SiO_2; Au−Au coordination number for Au/Al_2O_3. [c] ΔR is the difference between the metal−metal distance calculated for the sample and that found for the corresponding metal foil. [d] $3 < k < 8$ Å^{-1}.

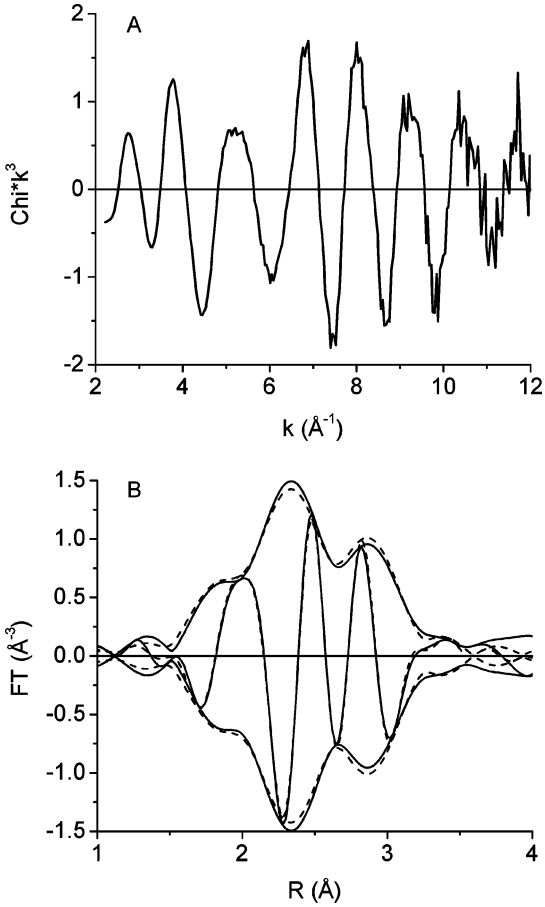

Figure 2. (A) k^3-weighted EXAFS function of Au/Al_2O_3-D after reduction and subsequent evacuation at 473 K and (B**)** corresponding Fourier transform (solid line) with best fit (dashed line) (R-space k^3 weighted fit, $1.5 < R < 3.5$ Å, $3 < k < 12$ Å^{-1}). The fit parameters are presented in Table 2.

Table 2 gives the results of the EXAFS analyses of the samples measured in a vacuum and in hydrogen atmosphere. The coordination numbers in a vacuum were used to determine the metal particle sizes (Table 1), assuming spherical particles.[35] Figure 2 shows the EXAFS function and its Fourier transform, including the best fit, of Au/Al_2O_3-D. Pt−O and Au−O contributions of about 0.1 oxygen neighbors per metal atom could be fitted, but the amount is considered below significance. For metal particles of 1 nm, a metal−oxygen coordination number (CN) of not more than 0.5 is expected, assuming that a metal atom in contact with the support has two oxygen neighbors. For bigger particles, the expected metal−oxygen CN

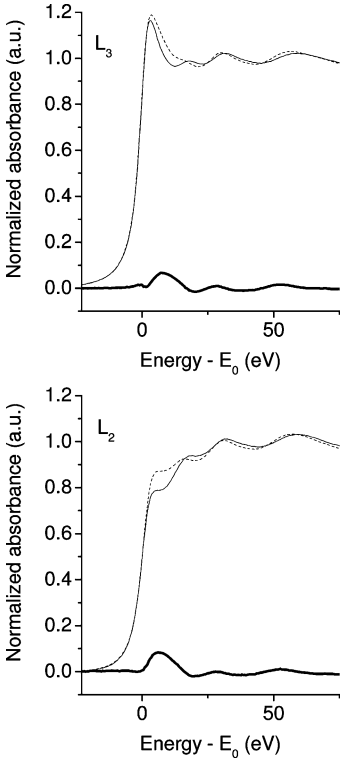

Figure 3. Pt L_3 and L_2 edges of Pt/SiO_2-A at 298 K measured in hydrogen after reduction at 473 K (dashed line), in dynamic vacuum after hydrogen removal by evacuation at 473 K (solid line), and their difference (bold solid line).

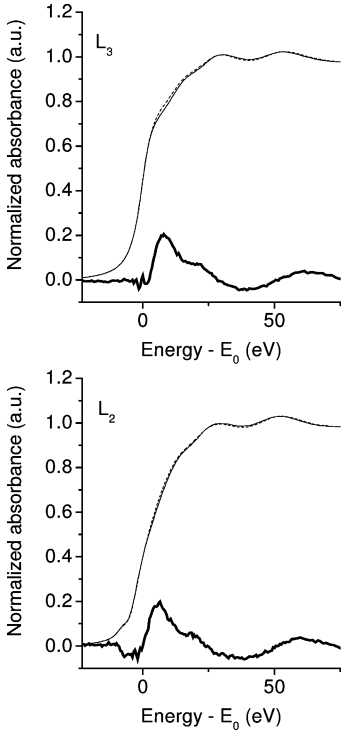

Figure 4. Au L_3 and L_2 edges of Au/Al_2O_3-D at 298 K measured in hydrogen after reduction at 473 K (dashed line), in dynamic vacuum after hydrogen removal by evacuation at 473 K (solid line), and their difference multiplied by 10 (bold solid line).

is even lower. The interatomic distances in both the Pt and Au samples are shorter than in the bulk, as expected for small particles. This contraction of the distances in small particles has been attributed to the higher electron density between the atoms because of dehybridization of the spd metal orbitals.[36] This effect increases with decreasing particle size. The Pt−Pt interatomic distance of the small Pt particles increases upon chemisorption of hydrogen because of the electron-withdrawing properties of hydrogen.[37] For Au/Al_2O_3, no effect of hydrogen adsorption on the Au−Au interatomic distance was observed.

XANES. The Pt L_3 and L_2 edges of Pt/SiO_2-A in hydrogen and in a vacuum are shown in Figure 3. Because of the chemisorption of hydrogen, large differences occur in both edges that are similar to those previously shown in the literature.[15−31] Figure 4 shows the $L_{3,2}$ edges of Au/Al_2O_3-D collected in hydrogen and in a vacuum. Upon the addition of hydrogen, there is a change in both edges between 0 and 25 eV over the edge. This range is the same as where the changes in the Pt edges appear. The hydrogen-induced effects on the L_3 and L_2 edges are depicted in Figure 5. These plots are obtained by subtracting the L_3 and L_2 edges in a vacuum from those in hydrogen, after the alignment as described in the Experimental Section. Figure 5A shows the hydrogen-induced effects for the two Pt/SiO_2 samples with either small or big platinum particles and Figure 5B for two Au/Al_2O_3 samples with different gold particle sizes. The effect on the $L_{3,2}$ edges of Pt/SiO_2 increases with decreasing particle size, because more Pt atoms form bonds with hydrogen. For Au too, the H-induced effect increases with decreasing particle size, and the extent of the change in the edges is smaller than for Pt.

Hydrogen Chemisorption. Table 3 lists the results of the hydrogen chemisorption analyses at various temperatures. The H/M of the total adsorption is determined from the first adsorption isotherm. The strong adsorption is determined from

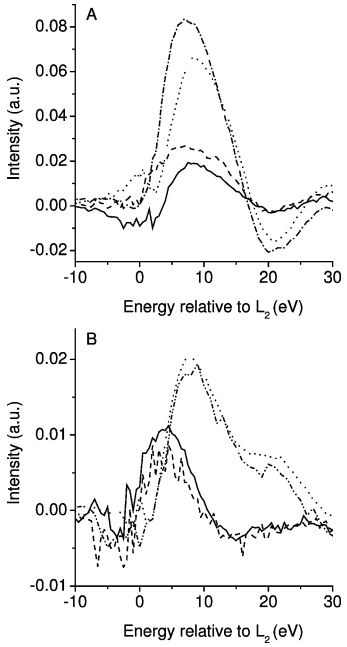

Figure 5. (A) Differences in the Pt L_3 and L_2 XANES between the spectra measured in a vacuum and in hydrogen (298 K): Pt/SiO_2-A L_3 (dotted line), Pt/SiO_2-A L_2 (dashed−dotted line), Pt/SiO_2-B L_3 (solid line), Pt/SiO_2-B L_2 (dashed line). (B) Differences in the Au L_3 and L_2 edges of the spectra measured in a vacuum and in hydrogen (298 K): Au/Al_2O_3-D L_3 (dotted line), Au/Al_2O_3-D L_2 (dashed−dotted line), Au/Al_2O_3-C L_3 (solid line), Au/Al_2O_3-C (dashed line).

the difference between the first and second adsorption isotherm and is the amount of hydrogen that does not desorb during the 2 h of evacuation at the analysis temperature. H/M values of at least 10% and as high as 73% were determined for the Au/Al_2O_3 catalysts. On Pt, the total amount of adsorbed hydrogen decreases with increasing temperature. In contrast, the hydrogen

TABLE 3: H/M Values of the Total and Strong Adsorption

sample	T (K)	H/M total adsorption	H/M strong adsorption[a]
Pt/SiO_2-A	298	121%	57%
	373	117%	27%
	423	105%	19%
	473	86%	
Pt/SiO_2-B	298	28%	12%
	373	25%	4%
	423	23%	2%
	473	20%	
Au/Al_2O_3-A	298	41%	3%
	373	50%	8%
	473	47%	
	523	50%	
Au/Al_2O_3-B	298	10%	3%
	373	16%	4%
Au/Al_2O_3-C	298	27%	6%
	373	27%	4%
	473	27%	
Au/Al_2O_3-D	298	66%	16%
	373	73%	18%
Au/Al_2O_3-E	298	41%	4%

[a] Strongly adsorbed hydrogen that does not desorb during 2 h evacuation at the analysis temperature.

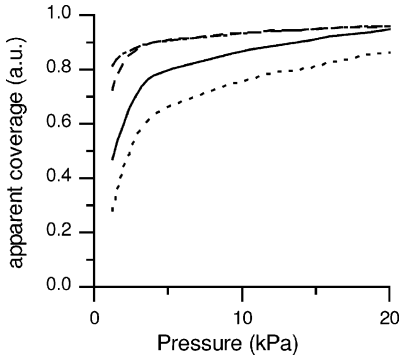

Figure 6. Hydrogen chemisorption isotherms of Pt/SiO_2-A (dashed−dotted line), Pt/SiO_2-B (dashed line), Au/Al_2O_3-D (solid line), and Au/Al_2O_3-A (dotted line), at 298 K. The apparent coverage for each catalyst is determined by taking the ratio of the amount of adsorbed hydrogen at a certain pressure to that at 100 kPa. The amounts at 100 kPa correspond to the H/M values as listed in Table 3.

adsorption on Au/Al_2O_3 increases or is constant from 298 to 523 K. On supported Pt, about half the adsorbed hydrogen is strongly adsorbed at 298 K. This fraction decreases with temperature, because a larger part of the adsorbed hydrogen desorbs at higher temperature. On Au/Al_2O_3, the strongly adsorbed hydrogen is 10−30% of the total amount.

Figure 6 gives the chemisorption isotherms at 298 K. The apparent coverage is determined by taking the ratio of the amount of adsorbed hydrogen at a certain pressure to that at 100 kPa. This is not the real coverage, since the amount of adsorbed hydrogen at 100 kPa depends on the temperature. A higher hydrogen pressure is necessary for supported gold than for supported Pt to obtain the same apparent coverage.

H/D Exchange. Table 4 presents the results of the H/D exchange experiments. The HD concentration is the ratio of the amount of HD (in mL/min) to the total amount of H_2, D_2, and HD in the product feed. The approach to equilibrium (η, eqs 1 and 2) is listed in the fourth column. The forward turnover frequencies (TOF) are calculated from the net turnover frequencies using the fractional distance from equilibrium (eqs 3 and 4). In the fifth column, the TOF per metal surface atom is listed. The TOF per hydrogen-adsorbing metal atom, as determined in the hydrogen chemisorption experiments, is given in the last column. The last value could not be determined at 338 K, because no hydrogen chemisorption experiments were done at this temperature. Over a supported Pt catalyst, a product mixture of 26% H_2, 26% D_2, and 47% HD was obtained. Thus, equilibrium is reached ($\eta = 1$) under the applied conditions, and the forward turnover frequency cannot be determined. Over Au/Al_2O_3-B, the product mixture contains 4% HD at room temperature. The HD concentration increases with increasing temperature, reaching 35% at 373 K, corresponding to an approach to equilibrium of $\eta = 0.36$. The concentration of HD obtained over Au/Al_2O_3-D is 1% at room temperature, corresponding to an η of 2.0×10^{-4}. This is an order of magnitude higher than over the bare Al_2O_3 support. At 373 K, the approach to equilibrium for Au/Al_2O_3-D reaches 0.18. The turnover frequencies increase with temperature. The TOF per available Au surface atom is similar for the two Au/Al_2O_3 samples. Over Au/Al_2O_3-B, more hydrogen molecules are converted per hydrogen-adsorbing Au atom.

Discussion

Adding hydrogen to Au/Al_2O_3 induced a change in the Au L_3 and L_2 X-ray absorption near-edge structures, similar to the change that occurred in the Pt $L_{3,2}$ edges. Thus, hydrogen chemisorbs on gold particles supported on Al_2O_3. Furthermore, in-situ XAS is a good tool for obtaining hydrogen-binding sites on supported gold catalysts.[30]

The shape of the hydrogen adsorption isotherms is typical for strong adsorption. As found with density functional theory (DFT) calculations, the strength of the molecular adsorption of hydrogen molecules on gold clusters of 1 nm is only −3 kJ/mol, whereas the adsorption energy of hydrogen atoms is −250 kJ/mol.[38] This implies that hydrogen is dissociatively adsorbed on supported gold catalysts, which is also proved in H/D exchange tests. In the adsorption experiments, a lower hydrogen uptake is measured after increasing the gold particle size by high-temperature reduction (Au/Al_2O_3-D to Au/Al_2O_3-E). This effect of particle size on the hydrogen uptake confirms the results of in-situ XAS, which showed that the hydrogen atoms adsorb on the gold particles. The average number of hydrogen atoms chemisorbed per surface metal atom can be determined by comparing the H/M values with the metal particle sizes. Assuming spherical particles, the metal particle sizes, as determined with EXAFS and STEM, are converted to EXAFS

TABLE 4: HD Concentration in the Product Feed, Approach to Equilibrium (η), and Forward Turnover Frequencies (TOF) in the H/D Exchange Experiments

sample	T (K)	HD concentration	η	TOF (mol/mol surface atom/min)	TOF (mol/mol H/M site/min)
Al_2O_3	298	0.6%	3.9×10^{-5}		
	373	1.3%	2.1×10^{-4}		
$Pt/SiO_2/Al_2O_3$	298	47%	1		
Au/Al_2O_3-B	298	4%	2.5×10^{-3}	4	29
	338	20%	7.4×10^{-2}	17	
	373	35%	3.6×10^{-1}	46	213
Au/Al_2O_3-D	298	1%	2.0×10^{-4}	3	4
	338	13%	2.6×10^{-2}	28	
	373	27%	1.8×10^{-1}	60	88

and STEM dispersions.[39] The platinum particle size in Pt/SiO_2−A is 1.2−2 nm, corresponding to a dispersion of 60−80%. A H/Pt of around 120% was found at 298 and 373 K. On these small particles, more than one hydrogen atom can be chemisorbed per Pt surface atom,[39] probably on the corners and edges. For the bigger Pt particles, the H/Pt value and the EXAFS dispersion are in agreement; thus, on average, one H atom is adsorbed per Pt surface atom. The H/Au values of the gold catalysts are up to 5 times lower than the EXAFS and STEM dispersions; per surface Au atom, 0.2−0.8 hydrogen atoms are adsorbed. The $H/Au_{surface}$ value of 0.4 found for Au/Al_2O_3 that is active in acetylene hydrogenation lies in the same range.[5] Au/Al_2O_3−D has the smallest gold particles and the highest $H/Au_{surface}$. For particles of 1 nm, as in this sample, all surface atoms are on corner and edge positions, whereas for particles of 1.5 nm, 20% of the surface atoms are at face positions.[40] It seems that the hydrogen atoms only adsorb on Au atoms at corner and edge positions. On platinum, the atoms at the corners and edges dissociate hydrogen, which then spills over onto the Pt atoms at the faces.[41] In this way, all the surface Pt atoms are covered by hydrogen. For Ag particles supported on SiO_2, it was recently proposed that hydrogen dissociation occurs at defect sites or kinks, and the hydrogen atoms may then diffuse onto the flat surfaces.[42] We suggest that, on gold, the hydrogen atoms do not spill over onto the face sites after dissociation. As described in the Introduction, thin films consisting of gold islands dissociate and chemisorb hydrogen, but the hydrogen coverage is low.[12] Okada et al. ascribed the dissociative adsorption of hydrogen on thin gold films grown on Ir(111) only to localized sites, such as defects and steps originating from strain.[13] For the oxygen activation on Au surfaces, it was shown that steps and lattice expansion substantially facilitate O_2 activation.[43] With DFT calculations, Mavrikakis et al.[44] showed that strain effects and higher step densities increase the reactivity of gold surfaces. In the crotonaldehyde hydrogenation over Au/TiO_2, the turnover frequency (in number of converted molecules per gold surface atom per second) dramatically increases when the gold particle size decreases to below 2 nm.[10] These authors suggest that the rate-determining step in this reaction is the dissociation of hydrogen, which occurs on gold atoms at edges and corners. In acrolein hydrogenation, the higher activity of Au/TiO_2 compared to Au/ZrO_2 was attributed to the high fraction of corners and edges on the gold particles on TiO_2; on ZrO_2, the particles were facetted.[7] These studies support our proposal: hydrogen is dissociated on corners and edges and subsequently interacts with other reactants without diffusing to face sites. The absence of spillover onto nondissociating gold atoms means that hydrogen chemisorption is not a suitable technique for determining the size of gold particles, however, it is suitable for studying the gold atoms on corner and edge positions.

The amount of hydrogen adsorbed on the supported Pt particles decreases with temperature, because the equilibrium shifts toward hydrogen in the gas phase. In contrast, the H/Au of the gold nanoparticles does not decrease with temperature. Considering thermodynamics, the amount of adsorbed hydrogen should decrease with temperature, as for Pt. Thus, on gold, kinetic factors also play a role. The increase in the amount of adsorbed hydrogen with temperature is caused by the hydrogen dissociation over gold nanoparticles being activated. Lin and Vannice[14] also suggested that activated dissociation and adsorption of hydrogen occurs on gold particles and others suggested that O_2 dissociation on gold is an activated process.[43] For the Au/Al_2O_3 catalysts in our study, the adsorption is limited by kinetic factors from 298 to 373 K. It is expected that at higher temperatures thermodynamic factors will be limiting and that at a certain temperature the hydrogen uptake will reach a maximum.

To obtain the same apparent hydrogen coverage, a higher pressure is necessary for supported gold than for platinum. Furthermore, on Au particles, a smaller fraction of the adsorbed hydrogen is strongly adsorbed than on Pt particles of similar size. Also, the intensity of the H-induced effect on the Au $L_{3,2}$ edges is smaller than on the Pt $L_{3,2}$ edges for samples with similar H/M values. This suggests that the interaction of hydrogen with gold is weaker than the hydrogen−Pt interaction. It is not possible to determine the strength of the hydrogen−gold interaction by calculating the adsorption equilibrium constants, because on gold the adsorption process is not in equilibrium.

Isotope exchange occurs in the H/D exchange experiments, confirming that the Au/Al_2O_3 catalysts dissociate hydrogen. Equilibrium is not reached under the applied conditions, whereas it is reached by supported Pt catalysts. It has been reported that, over Pt particles, complete equilibration is reached at temperatures as low as 77 K.[45−47] Au/Al_2O_3−B, having bigger gold particles, comes closer to equilibrium than Au/Al_2O_3−D. The turnover frequency per gold surface site is the same for these two Au/Al_2O_3 catalysts. Per hydrogen-adsorbing site, the turnover frequency is higher over Au/Al_2O_3−B. A direct comparison between these two catalysts is not feasible, since they differ not only in particle size and gold content but also in the method of preparation. The preparation method can influence the activity.[2−4] Nevertheless, these experiments prove that Au/Al_2O_3 catalysts, with Au particle sizes of 1−3 nm, prepared by deposition−precipitation or incipient wetness impregnation, dissociate hydrogen. The HD concentration increases with temperature. This is caused by two effects. The first is the increase in hydrogen coverage with temperature because of the activated dissociation of hydrogen. The second effect is the increase in the rate constant for recombination. This explains why the increase in HD formation is stronger than the increase in the H/Au values. Moreover, it explains the small amount of HD at 298 K as opposed to the high hydrogen coverage found for chemisorption; at this temperature, the recombination rate is low.

For the dissociation of oxygen on thin gold films, it was found that impurities such as Si, Ag, and In dissociate oxygen, which then spills over onto the gold.[11,48−50] Here, it could be that impurities such as Pt dissociate hydrogen, which then spills over onto the gold. However, no Pt was detected by X-ray absorption spectroscopy, meaning that the Pt level is well below 1% that of gold. The level of impurities in the $HAuCl_4$ that was the precursor is 0.1%. The probable role of possible impurities cannot be ruled out, nevertheless, the supported gold samples exhibit unique properties: the increase of the capacity to dissociate hydrogen and the hydrogen uptake with increasing temperature. If gold only chemisorbs hydrogen atoms supplied by another metal like Pt, then the hydrogen uptake would decrease with increasing temperature.

The dissociation and chemisorption of hydrogen is an essential first step in hydrogenation reactions. We showed that gold particles supported on Al_2O_3 dissociate and chemisorb hydrogen and that this process is activated. Small particles, with a diameter of a few nanometers, are required, because those have a large fraction of gold atoms on corners and edges. The interaction of hydrogen with supported gold is weaker than with Pt, and the interaction is limited to corners and edges. Therefore, supported gold nanoparticles will perform differently in catalysis

compared to supported platinum catalysts. The weakly bound hydrogen can react easily with other adsorbates, even at low temperature, at which competitive reaction pathways leading to byproducts are suppressed. Thus, even though supported gold catalysts might have a lower activity than conventional hydrogenation catalysts, the selectivity could be increased. Selective catalysts for low-temperature hydrogenation reactions are of special interest in the production of fine chemicals.[51] The successful use of supported gold nanoparticles to selectively hydrogenate acetylene,[5] 1,3-butadiene, acrolein, crotonaldehyde,[6−8] and other α,β-unsaturated aldehydes[9,10] has been shown. The performance of gold catalysts in, for example, the acrolein hydrogenation is comparable to that of supported silver nanoparticles that also exhibit a weak and structure-sensitive interaction with hydrogen.[42] The selective hydrogenation of acetylene to ethylene takes place from 313 to 523 K, and at 573 K, ethane also forms.[5] This can be explained by a higher coverage of the reactants at higher temperature. The low hydrogen coverage on gold nanoparticles implies that hydrogen is rate-limiting, as proposed on the basis of catalytic studies.[10] Moreover, gold will probably be less active than Pt in the activation of C−H and C−C bonds. Therefore, less hydrogenolysis at high temperature is expected to occur. The weak H−Au bonding and low coverage make supported Au catalysts promising for high-temperature dehydrogenation, with little byproduct and coke formation.

Conclusion

Hydrogen dissociatively adsorbs on the gold atoms of Au/Al_2O_3 catalysts prepared by impregnation and deposition−precipitation. The dissociation and adsorption of hydrogen is limited to the gold atoms on corner and edge positions. The hydrogen dissociation by gold is activated; both the activity in H/D exchange and the hydrogen uptake increase with temperature. The chemisorption of hydrogen induces changes in the Au L_3 and L_2 X-ray absorption near-edge structures, similar to the hydrogen-induced effect on the Pt L_3 and L_2 edges.

Acknowledgment. The authors thank Hasylab (Hamburg, Germany) and the European Synchrotron Radiation Facility (Grenoble, France) for the use of the synchrotron radiation facilities and the staff of Station X1 at Hasylab (Project number I-03-026), the Swiss-Norwegian Beamlines at the ESRF (Experiment number 01-01-661), and the Dutch-Belgian Beamline at the ESRF (Experiment number CH-1789). Dr. Frank Krumeich is thanked for the STEM measurements, Pijus Kanti Roy for support with the H/D exchange experiments, and Prof. dr. Roel Prins for valuable discussion. The Swiss National Science Foundation funded this work (Nr. 2-77264-03).

References and Notes

(1) Hammer, B.; Nørskov, J. K. *Nature* **1995**, *376*, 238−240.
(2) Haruta, M. *Catal. Today* **1997**, *36*, 153−166.
(3) Bond, G. C.; Thompson, D. T. *Catal. Rev.−Sci. Eng.* **1999**, *41*, 319−388.
(4) Haruta, M.; Daté, M. *Appl. Catal., A.: Gen.* **2001**, *222*, 427−437.
(5) Jia, J.; Haraki, K.; Kondo, J. N.; Domen, K.; Tamaru, K. *J. Phys. Chem. B* **2000**, *104*, 11153−11156.
(6) Schimpf, S.; Lucas, M.; Mohr, C.; Rodemerck, U.; Brückner, A.; Radnik, J.; Hofmeister, H.; Claus, P. *Catal. Today* **2002**, *72*, 63−78.
(7) Mohr, C.; Hofmeister, H.; Claus, P. *J. Catal.* **2003**, *213*, 86−94.
(8) Mohr, C.; Hofmeister, H.; Radnik, J.; Claus, P. *J. Am. Chem. Soc.* **2003**, *125*, 1905−1911.
(9) Milone, C.; Tropeano, M. L.; Guline, G.; Neri, G.; Ingoglia, R.; Galvagno, S. *Chem. Commun.* **2002**, 868−869.
(10) Zanella, R.; Louis, C.; Giorgio, S.; Touroude, R. *J. Catal.* **2004**, *223*, 328−339.
(11) Sault, A. G.; Madix, R. J.; Campbell, C. T. *Surf. Sci.* **1986**, *169*, 347−356.
(12) Stobiński, L.; Zommer, L.; Duś, R. *Appl. Surf. Sci.* **1999**, *141*, 319−325.
(13) Okada, M.; Nakamura, M.; Moritani, K.; Kasai, T. *Surf. Sci.* **2003**, *523*, 218−230.
(14) Lin, S.; Vannice, M. A. *Catal. Lett.* **1991**, *10*, 47−62.
(15) Samant, M. G.; Boudart, M. *J. Phys. Chem.* **1991**, *95*, 4070−4074.
(16) Ichikuni, N.; Iwasawa, Y. *Catal. Lett.* **1993**, *20*, 87−95.
(17) Otten, M. M.; Clayton, M. J.; Lamb, H. H. *J. Catal.* **1994**, *149*, 211−222.
(18) Vaarkamp, M.; Mojet, B. L.; Kappers, M. J.; Miller, J. T.; Koningsberger, D. C. *J. Phys. Chem.* **1995**, *99*, 16067−16075.
(19) Vaarkamp, M.; Miller, J. T.; Modica, F. S.; Koningsberger, D. C. *J. Catal.* **1996**, *163*, 294−305.
(20) Kubota, T.; Asakura, K.; Ichikuni, N.; Iwasawa, Y. *Chem. Phys. Lett.* **1996**, *256*, 445−448.
(21) Asakura, K.; Kubota, T.; Ichikuni, N.; Iwasawa, Y. *Stud. Surf. Sci. Catal.* **1996**, *101*, 911−919.
(22) Reifsnyder, S. N.; Otten, M. M.; Sayers, D. E.; Lamb, H. H. *J. Phys. Chem. B* **1997**, *101*, 4972−4977.
(23) Asakura, K.; Kubota, T.; Chun, W.-J.; Iwasawa, Y.; Ohtani, K.; Fujikawa, T. *J. Synchrotron Radiat.* **1999**, *6*, 439−441.
(24) Ramaker, D. E.; Mojet, B. L.; Garriga Oostenbrink, M. T.; Miller, J. T.; Koningsberger, D. C. *Phys. Chem. Chem. Phys.* **1999**, *1*, 2293−2302.
(25) Koningsberger, D. C.; Oudenhuijzen, M. K.; Bitter, J. H.; Ramaker, D. E. *Top. Catal.* **2000**, *10*, 167−177.
(26) Ankudinov, A. L.; Rehr, J. J.; Low, J. J.; Bare, S. R. *J. Synchrotron Radiat.* **2001**, *8*, 578−580.
(27) Ankudinov, A. L.; Rehr, J. J.; Low, J.; Bare, S. R. *Phys. Rev. Lett.* **2001**, *86*, 1642−1645.
(28) Ankudinov, A. L.; Rehr, J. J.; Low, J.; Bare, S. R. *Phys. Rev. Lett.* **2002**, *89*, 139702.
(29) Ramaker, D. E.; Koningsberger, D. C. *Phys. Rev. Lett.* **2002**, *89*, 139701.
(30) Koningsberger, D. C.; Oudenhuijzen, M. K.; de Graaf, J.; van Bokhoven, J. A.; Ramaker, D. E. *J. Catal.* **2003**, *216*, 178−191.
(31) Oudenhuijzen, M. K.; van Bokhoven, J. A.; Miller, J. T.; Ramaker, D. E.; Koningsberger, D. C. *J. Am. Chem. Soc.* **2005**, *127*, 1530−1540.
(32) Vaarkamp, M.; Linders, J. C.; Koningsberger, D. C. *Phys. B* **1995**, *208−209*, 159−160.
(33) Koningsberger, D. C.; Mojet, B. L.; van Dorssen, G. E.; Ramaker, D. E. *Top. Catal.* **2000**, *10*, 143−155.
(34) Zabinsky, S. I.; Rehr, J. J.; Ankudinov, A.; Albers, R. C.; Eller, M. J. *Phys. Rev. B* **1995**, *52*, 2995−3009.
(35) de Graaf, J.; van Dillen, A. J.; de Jong, K. P.; Koningsberger, D. C. *J. Catal.* **2001**, *203*, 307−321.
(36) Delley, B.; Ellis, D. E.; Freeman, A. J.; Baerends, E. J.; Post, D. *Phys. Rev. B* **1983**, *27*, 2132−2144.
(37) Sanchez Marcos, E.; Jansen, A. P. J.; van Santen, R. A. *Chem. Phys. Lett.* **1990**, *167*, 399−406.
(38) Barton, D. G.; Podkolzin, S. G. *J. Phys. Chem. B* **2004**, *109*, 2262−2274.
(39) Kip, B. J.; Duivenvoorden, F. B. M.; Koningsberger, D. C.; Prins, R. *J. Catal.* **1987**, *105*, 26−38.
(40) van Hardeveld, R.; Hartog, F. *Surf. Sci.* **1969**, *15*, 189−230.
(41) Bernasek, S. L.; Somorjai, G. A. *J. Chem. Phys.* **1975**, *62*, 3149−3161.
(42) Bron, M.; Kondratenko, E.; Trunschke, A.; Claus, P. *Z. Phys. Chem.* **2004**, *218*, 405−423.
(43) Xu, Y.; Mavrikakis, M. *J. Phys. Chem. B* **2003**, *107*, 9298−9307.
(44) Mavrikakis, M.; Stoltze, P.; Nørskov, J. K. *Catal. Lett.* **2000**, *64*, 101−106.
(45) Susumu, T.; Yoshimitsu, A.; Ratimer, J. C. *J. Catal.* **1971**, *20*, 1−9.
(46) Nishiyama, S.; Yoshida, T.; Kimura, K.; Tsuruya, S.; Masai, M. *Catal. Today* **1996**, *28*, 205−214.
(47) Novakova, J.; Brabec, L. *J. Catal.* **1997**, *166*, 186−194.
(48) Canning, N. D. S.; Outka, D.; Madix, R. J. *Surf. Sci.* **1984**, *141*, 240−254.
(49) Pireaux, J. J.; Chtaïb, M.; Delrue, J. P.; Thiry, P. A.; Liehr, M.; Caudano, R. *Surf. Sci.* **1984**, *141*, 221−232.
(50) Iizuka, Y.; Kawamoto, A.; Akita, K.; Daté, M.; Tsubota, S.; Okumura, M.; Haruta, M. *Catal. Lett.* **2004**, *97*, 203−208.
(51) Greeley, J.; Mavrikakis, M. *Nat. Mater.* **2004**, *3*, 810−815.